

# Active RIS vs. Passive RIS: Which Will Prevail in 6G?

Zijian Zhang, Linglong Dai, Xibi Chen, Changhao Liu, Fan Yang, Robert Schober, and H. Vincent Poor

**Abstract**—As a revolutionary paradigm for controlling wireless channels, reconfigurable intelligent surfaces (RISs) have emerged as a candidate technology for future 6G networks. However, due to the “multiplicative fading” effect, RISs only achieve a negligible capacity gain in many scenarios with strong direct links. In this paper, the concept of active RISs is proposed to overcome this fundamental limitation. Unlike the existing passive RISs that reflect signals without amplification, active RISs can amplify the reflected signals. We develop a signal model for active RISs, which is validated through experimental measurements. Based on this model, we formulate the sum-rate maximization problem for active RIS aided multiple-input multiple-output (MIMO) systems and a precoding algorithm is proposed to solve this problem. Results show that, in a typical wireless system, the existing passive RISs can realize only a negligible sum-rate gain of 3%, while the proposed active RISs can achieve a significant sum-rate gain of 108%, thus overcoming the “multiplicative fading” effect.

**Index Terms**—Reconfigurable intelligent surface (RIS), beam-forming, active RIS, signal model.

## I. INTRODUCTION

As wireless communications have advanced from the first generation (1G) to 5G, the system capacity has been significantly increased by improving the transceiver design, while the wireless channels have been usually considered to be uncontrollable. Recently, due to advances in meta-materials, reconfigurable intelligent surfaces (RISs) have been proposed [1]–[4] for the purpose of intelligently controlling wireless channels for improved communication performance. Specifically, an RIS is an array composed of a very large number of passive elements that reflects electromagnetic signals in a desired manner so as to reconfigure the propagation properties of the wireless environment [5]. Thanks to their high array gain, low cost, low power, and low noise [5]–[7], RISs promise to improve channel capacity [8], extend coverage [9], and save

power [10] in future 6G networks. Additionally, RISs are also projected to have other applications such as in WiFi [11], precision measurement [12], and navigation [13].

The negligible noise introduced by passive RISs enables a “square-law” array gain. In particular, the array gain of an  $N$ -element RIS is proportional to  $N^2$ , which is  $N$  times larger than that achievable by standard massive multiple-input multiple-output (MIMO) systems [5]. Benefiting from this advantage, RISs are expected to introduce significant capacity gains [8]. However, in practice, these capacity gains are typically only observed in communication scenarios where the direct link between transmitter and receiver is completely blocked or very weak [8]–[10], [14]–[16]. By contrast, in many scenarios where the direct link is not weak, common RISs can achieve only negligible capacity gains [17]. The reason behind this phenomenon is the “multiplicative fading” effect introduced by RISs, i.e., the equivalent path loss of the transmitter-RIS-receiver link is the product (instead of the sum) of the path losses of the transmitter-RIS link and RIS-receiver link, which is usually thousands of times larger than that of the direct link [17]. As a result, the “multiplicative fading” effect makes it almost impossible for passive RISs to achieve noticeable capacity gains in many wireless environments. Many existing works on RISs have bypassed this effect by only considering scenarios with very poor direct links [8]–[10], [14]–[16]. Therefore, to advance the practicability of RISs in future 6G wireless networks, a critical issue to be addressed is: *How to overcome the fundamental performance bottleneck caused by the “multiplicative fading” effect of RISs.*

To overcome the fundamental physical limitation imposed by the “multiplicative fading” effect, the new concept of active RIS is proposed in this paper. Specifically, our contributions are summarized as follows:

- We propose the concept of *active* RISs to overcome the “multiplicative fading” effect. Different from the existing *passive* RISs that just passively reflect signals without amplification, the key feature of active RISs is their capability of actively reflecting signals with amplification at the expense of additional power consumption.
- We develop a new signal model for the proposed active RISs, which characterizes the amplification of the incident signal and incorporates the non-negligible thermal noise introduced by the active elements. For verification, an active RIS element was designed and fabricated to validate the developed signal model through experimental measurements.
- Based on the proposed signal model, we formulate a sum-rate maximization problem for an active RIS aided MIMO

Z. Zhang, L. Dai, X. Chen, C. Liu, and F. Yang are with the Department of Electronic Engineering as well as the Beijing National Research Center for Information Science and Technology (BNRist), Tsinghua University, Beijing 100084, China (e-mails: zhangzijian15@mails.tsinghua.edu.cn, daill@tsinghua.edu.cn, cxb17@mails.tsinghua.edu.cn, liuch17@mails.tsinghua.edu.cn, fan\_yang@tsinghua.edu.cn).

R. Schober is with the Institute for Digital Communications at Friedrich-Alexander University Erlangen-Nürnberg (FAU) (e-mail: robert.schober@fau.de).

H. V. Poor is with the Department of Electrical and Computer Engineering, Princeton University, USA (e-mail: poor@princeton.edu).

This work was supported in part by the National Key Research and Development Program of China (Grant No. 2020YFB1807201), in part by the National Natural Science Foundation of China (Grant No. 62031019), and in part by the U.S. National Science Foundation under Grants CCF-0939370 and CCF-1908308.

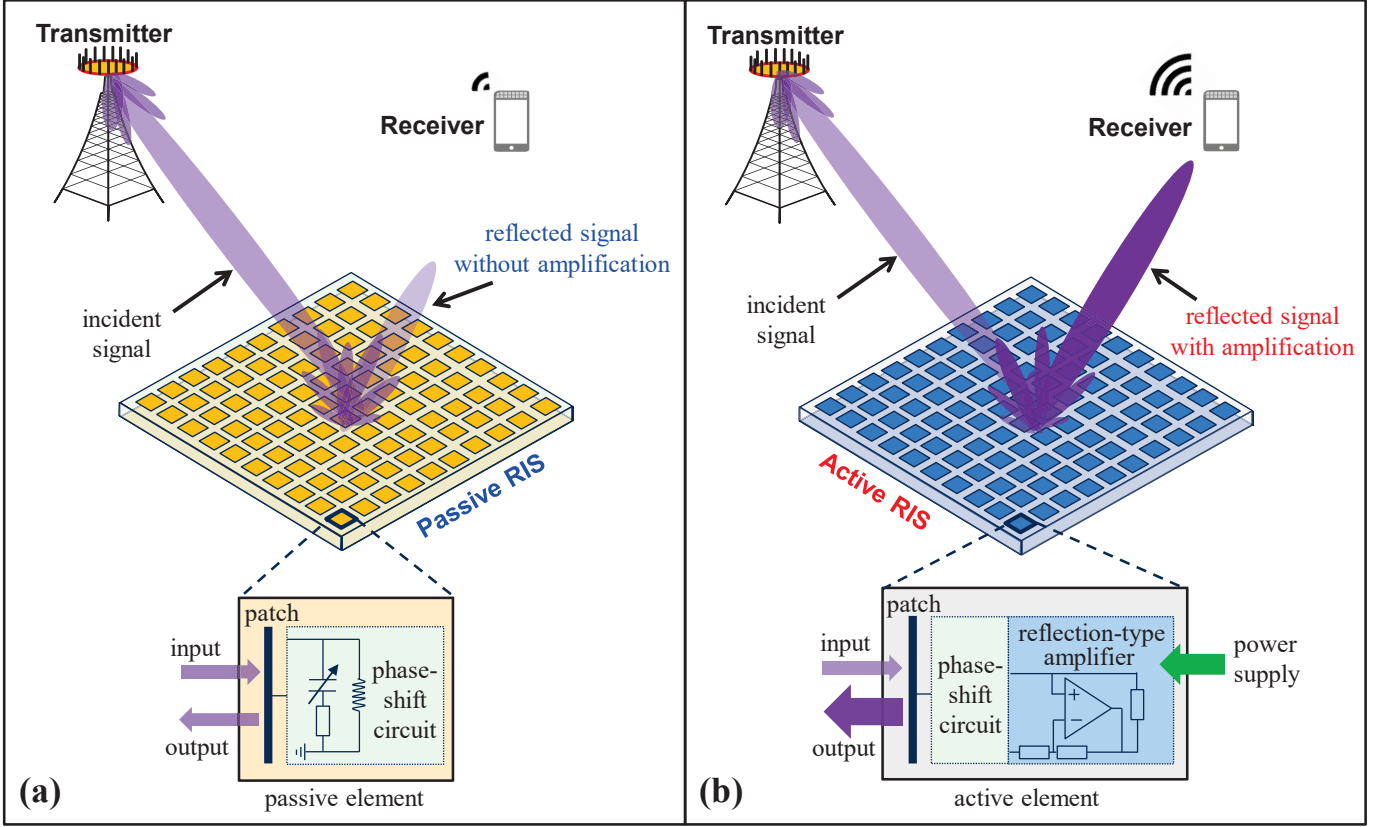


Fig. 1. Comparison between the existing passive RIS (a) and the proposed active RIS (b).

system, and present a joint transmit beamforming and reflect precoding algorithm that solves this problem. Our results show that, in a typical wireless system, the existing passive RISs achieve only a negligible sum-rate gain of 3%, while the proposed active RISs are able to achieve a noticeable sum-rate gain of 108%, thus overcoming the “multiplicative fading” effect.

The rest of this paper is organized as follows. The concept of active RISs is introduced in Section II, and its impact on channel capacity is analyzed in Section III. Then, the proposed precoding design for capacity maximization is provided in Section IV. In Section V, experimental measurements and numerical simulation results are presented. Finally, conclusions are drawn in Section VI.

*Notations:*  $\mathbb{C}$  and  $\mathbb{R}_+$  denote the sets of complex and positive real numbers, respectively;  $[\cdot]^{-1}$ ,  $[\cdot]^T$ , and  $[\cdot]^H$  denote the inverse, transpose, and conjugate-transpose operations, respectively;  $\|\cdot\|$  denotes the Frobenius norm of its argument;  $\text{diag}(\cdot)$  denotes the diagonal matrix of its argument;  $\Re\{\cdot\}$  denotes the real part of its argument;  $\otimes$  denotes the Kronecker product;  $\angle[\cdot]$  denotes the angle of its complex argument;  $\ln(\cdot)$  denotes the natural logarithm of its argument;  $\mathcal{CN}(\mu, \Sigma)$  denotes the complex multivariate Gaussian distribution with mean  $\mu$  and variance  $\Sigma$ ;  $\mathbf{I}_L$  is an  $L \times L$  identity matrix, and  $\mathbf{0}_L$  is an  $L \times 1$  zero vector.

## II. CONCEPT OF ACTIVE RIS

In this section, we propose the concept of active RISs. First, we review the existing passive RISs, and point out their fundamental limitation caused by the “multiplicative fading” effect. Then, to overcome this limitation, we propose the concept of active RISs along with their hardware structure and signal model. Finally, we present the transmission model for an active RIS aided MIMO system.

### A. Existing Passive RIS

The RISs widely studied in existing works are passive devices [1]–[10]. Specifically, as shown in Fig. 1 (a), a passive RIS comprises a large number of passive elements each being able to reflect the incident signal with a controllable phase shift. Each passive RIS element consists of a reflective patch terminated with an impedance-adjustable circuit for phase shifting [1], [4], [18]. Thanks to its passive operating mode, a passive RIS element practically consumes zero direct-current power [18], and the introduced thermal noise is also negligible [5]–[10]. Thereby, the signal model of an  $N$ -element passive RIS widely used in the literature is given as follows [6]

$$\mathbf{y} = \Theta \mathbf{x}, \quad (1)$$

where  $\mathbf{x} \in \mathbb{C}^N$  denotes the incident signal,  $\Theta \triangleq \text{diag}(e^{j\theta_1}, \dots, e^{j\theta_N}) \in \mathbb{C}^{N \times N}$  denotes the phase shift matrix of the RIS, and  $\mathbf{y} \in \mathbb{C}^N$  denotes the signal reflected by the RIS. Note that the impact of noise is neglected in (1). As

a consequence, by properly adjusting  $\Theta$  to manipulate the  $N$  signals reflected by the  $N$  RIS elements to coherently add with the same phase at the receiver, a high array gain proportional to  $N^2$  can be achieved. This is expected to significantly increase the receiver signal-to-noise ratio (SNR) [5]–[7], which is the key reason for why RISs have attracted so much research interest recently [8]–[16].

Unfortunately, in practice, this expected high capacity gain often cannot be achieved in communication scenarios where the direct link between the transmitter and the receiver is not weak. The reason for this result is the “multiplicative fading” effect, i.e., the equivalent path loss of the transmitter-RIS-receiver reflection link is the product (instead of the sum) of the path losses of the transmitter-RIS link and RIS-receiver link, and therefore, it is thousands of times larger than that of the unobstructed direct link. Thereby, for an RIS to realize a noticeable capacity gain, thousands of RIS elements are required to compensate for this extremely large path loss. For example, let us consider a single-input single-output (SISO) system aided by a passive RIS with an element spacing of a half wavelength [19]. Let  $d = 200$  m,  $d_t = 150$  m, and  $d_r = 200$  m denote the distances between transmitter and receiver, transmitter and RIS, RIS and receiver, respectively. For carrier frequencies of 5/10/20 GHz, according to the RIS “multiplicative fading” model [17],  $N = 10000/20000/40000$  RIS elements are required to make the reflection link as strong as the direct link. Due to the high signaling overhead introduced by the  $N$  pilots required for channel estimation [20] and the high complexity of  $\mathcal{O}(N^2)$  for real-time beam-forming [21], such a large number of RIS elements makes the application of passive RISs in practical wireless networks very challenging [17]. Consequently, many existing works have bypassed the “multiplicative fading” effect by only considering the scenario where the direct link is completely blocked or very weak [5]–[10], [14]–[16].

### B. Proposed Active RIS

To overcome the fundamental physical limitation of the “multiplicative fading” effect, we propose the concept of active RISs as a promising solution. As shown in Fig. 1 (b), similar to the existing passive RISs, active RISs can also reflect the incident signals with reconfigurable phase shifts. Different from passive RISs that just reflect signals without amplification, active RISs can further amplify the reflected signals. To achieve this goal, the key component of an active RIS element is the additionally integrated active reflection-type amplifier, which can be realized by different existing active components, such current-inverting converters [22], asymmetric current mirrors [23], or even some integrated circuits [24].<sup>1</sup>

With an amplifier supported by a power supply, the reflected and amplified signal of an  $N$ -element active RIS can be modeled as follows:

$$\mathbf{y} = \underbrace{\mathbf{P}\Theta\mathbf{x}}_{\text{Desired signal}} + \underbrace{\mathbf{P}\Theta\mathbf{v}}_{\text{Dynamic noise}} + \underbrace{\mathbf{n}_s}_{\text{Static noise}}, \quad (2)$$

<sup>1</sup>In this paper, we focus on studying reflective active RISs, while the investigation of transmissive active RISs is left for future work [25]–[27].

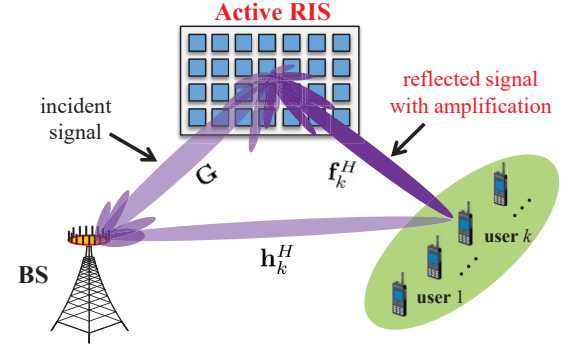


Fig. 2. An illustration of the downlink transmission in an active RIS aided MIMO system.

where  $\mathbf{P} \triangleq \text{diag}(p_1, \dots, p_N) \in \mathbb{R}_+^{N \times N}$  denotes the amplification factor matrix of the active RIS, wherein each element can be larger than one thanks to the integrated active amplifier. Due to the use of active components, active RISs consume additional power for amplifying the reflected signals, and the thermal noise introduced by active RIS elements cannot be neglected as is done for passive RISs. Particularly, as shown in (2), the introduced noise processes can be classified into dynamic noise and static noise [23]. Specifically,  $\mathbf{v}$  is related to the input noise and the inherent device noise of active RIS elements [23], while the static noise  $\mathbf{n}_s$  is unrelated to  $\mathbf{P}$  and is usually negligible compared to the dynamic noise  $\mathbf{P}\Theta\mathbf{v}$  [23]. Here, we neglect  $\mathbf{n}_s$  and model  $\mathbf{v}$  as  $\mathbf{v} \sim \mathcal{CN}(\mathbf{0}_N, \sigma_v^2 \mathbf{I}_N)$ .

Note that, the proposed active RISs are fundamentally different from the RISs equipped with active radio-frequency (RF) components [28]–[30]. Specifically, in [28]–[30], some passive RIS elements are connected to additional active RF chains, which are used for sending pilot signals and processing baseband signals. Thus, these RIS elements have signal processing capabilities [28]–[30], similar to full-duplex decode-and-forward (FD-DF) relays. On the contrary, the proposed active RISs do not have such capabilities but only reflect and amplify the incident signals to strengthen the reflection links. Besides, although the proposed active RISs can amplify the incident signals, similar to full-duplex amplify-and-forward (FD-AF) relays, the respective hardware structures and transmission models are quite different. Specifically, an FD-AF relay is equipped with RF chains to receive the incident signal and then transmit it after amplification [31]. Due to the long delay inherent to this process, two time slots are needed to complete the transmission of one symbol, and the received signal at the receiver in a time slot actually carries two different symbols, which are transmitted by the transmitter and the FD-AF relay, respectively [31]. In this way, in order to efficiently decode the symbols, the receiver in an FD-AF relay aided system has to combine the received signals in two adjacent time slots to maximize the SNR. Thus, FD-AF relaying involves two different transmission models in two adjacent time slots [31, Eq. (22), Eq. (25)], while the proposed active RIS follows the name transmission model (i.e., (3)) in each time slot, which also leads to different achievable rates [31, Table I].

### C. Active RIS Aided Downlink MIMO System

To evaluate the performance gains enabled by active RISs, we consider an active RIS aided downlink MIMO system as shown in Fig. 2, where an  $M$ -antenna base station (BS) simultaneously serves  $K$  single-antenna users with the aid of an  $N$ -element active RIS. Therefore, according to (2), the signal  $r_k \in \mathbb{C}$  received at user  $k$  can be modeled as

$$r_k = \underbrace{(\mathbf{h}_k^H)}_{\text{Direct link}} + \underbrace{(\mathbf{f}_k^H \mathbf{P} \mathbf{\Theta} \mathbf{G})}_{\text{Reflection link}} \sum_{j=1}^K \mathbf{w}_j s_j + \underbrace{(\mathbf{f}_k^H \mathbf{P} \mathbf{\Theta} \mathbf{v})}_{\text{Noise introduced by active RIS}} + \underbrace{z_k}_{\text{Noise introduced at user } k}, \quad (3)$$

where  $\mathbf{s} \triangleq [s_1, \dots, s_K]^T \in \mathbb{C}^K$  denotes the transmitted symbol vector for the  $K$  users with  $\mathbb{E}\{\mathbf{s}\mathbf{s}^H\} = \mathbf{I}_K$ ;  $\mathbf{G} \in \mathbb{C}^{N \times M}$ ,  $\mathbf{h}_k^H \in \mathbb{C}^{1 \times M}$ , and  $\mathbf{f}_k^H \in \mathbb{C}^{1 \times N}$  denote the channels from BS to RIS, from BS to user  $k$ , and from RIS to user  $k$ , respectively;  $\mathbf{w}_k \in \mathbb{C}^{M \times 1}$  denotes the BS beamforming vector for  $s_k$ ; and  $z_k$  denotes the additive white Gaussian noise (AWGN) at user  $k$  with  $z_k \sim \mathcal{CN}(0, \sigma^2)$ .

To illustrate how active RISs can overcome the “multiplicative fading” effect, based on the signal model in (2), the capacity gain achievable by active RISs will be analyzed in the next section.

### III. PERFORMANCE ANALYSIS

We analyze the capacity gain enabled by the use of an active RIS by studying the user’s achievable SNR in a simple SISO scenario. To focus on the capacity gain provided by the active RIS aided reflection link, we ignore the direct link by setting  $\mathbf{h}_k \triangleq \mathbf{0}$  [32]. For simplicity, we assume that every active RIS element has the same amplification factor ( $p_n \triangleq p$ ,  $\forall n \in \{1, \dots, N\}$ ), and redefine  $\mathbf{G} \triangleq \mathbf{g} = [g_1, \dots, g_N]^T$ ,  $\mathbf{f}_k \triangleq \mathbf{f} = [f_1, \dots, f_N]^T$ , and  $\mathbf{w}_k \triangleq \mathbf{w}$ . Then, we obtain the following lemma.

**Lemma 1:** Assuming  $\mathbf{f} \sim \mathcal{CN}(\mathbf{0}_N, \varrho_f^2 \mathbf{I}_N)$ ,  $\mathbf{g} \sim \mathcal{CN}(\mathbf{0}_N, \varrho_g^2 \mathbf{I}_N)$  and letting  $N \rightarrow \infty$ , the asymptotic SNR of an active RIS aided SISO system is

$$\gamma_{\text{active}} \rightarrow N \frac{P_{\text{BS}}^{\max} P_{\text{A}}^{\max} \pi^2 \varrho_f^2 \varrho_g^2}{16 \left( P_{\text{A}}^{\max} \sigma_v^2 \varrho_f^2 + P_{\text{BS}}^{\max} \sigma^2 \varrho_g^2 + \sigma^2 \sigma_v^2 \right)}, \quad (4)$$

where  $P_{\text{BS}}^{\max}$  and  $P_{\text{A}}^{\max}$  denote the maximum transmit power and reflect power at the BS and the active RIS, respectively.

*Proof:* In the considered active RIS aided SISO system, the downlink transmission model can be rewritten as

$$r = \underbrace{(\mathbf{f}^H \mathbf{P} \mathbf{\Theta} \mathbf{g})}_{\text{Reflection link}} \mathbf{w} s + \underbrace{(\mathbf{f}^H \mathbf{P} \mathbf{\Theta} \mathbf{v})}_{\text{Noise introduced by active RIS}} + \underbrace{z}_{\text{Noise introduced at user}}. \quad (5)$$

Thus, the maximization of the user’s SNR,  $\gamma$ , subject to the power constraints at the BS and the active RIS can be formulated as follows:

$$\max_{\mathbf{p}, \mathbf{\Theta}} \gamma = \frac{|p \mathbf{f}^H \mathbf{\Theta} \mathbf{g} \mathbf{w}|^2}{p^2 \|\mathbf{f}^H \mathbf{\Theta}\|^2 \sigma_v^2 + \sigma^2}$$

$$\text{s.t. } C_1 : |w|^2 \leq P_{\text{BS}}^{\max} \quad (6)$$

$$C_2 : p^2 \|\mathbf{\Theta} \mathbf{g} \mathbf{w}\|^2 + p^2 \|\mathbf{\Theta}\|^2 \sigma_v^2 \leq P_{\text{A}}^{\max},$$

where  $P_{\text{BS}}^{\max}$  and  $P_{\text{A}}^{\max}$  denote the maximum transmit power and reflect power at the BS and the active RIS, respectively.

The optimal solution of problem (6) can be obtained by the Lagrange multiplier method as

$$w^{\text{opt}} = \sqrt{P_{\text{BS}}^{\max}}, \quad (7a)$$

$$\theta_n^{\text{opt}} = \angle f_n - \angle g_n, \quad \forall n \in \{1, \dots, N\}, \quad (7b)$$

$$p^{\text{opt}} = \sqrt{\frac{P_{\text{A}}^{\max}}{P_{\text{BS}}^{\max} \sum_{n=1}^N |g_n|^2 + N \sigma_v^2}}. \quad (7c)$$

By substituting (7) into (6), the user’s maximum SNR for active RISs is obtained as follows

$$\gamma_{\text{active}} = \frac{P_{\text{BS}}^{\max} P_{\text{A}}^{\max} \left| \sum_{n=1}^N |f_n| |g_n| \right|^2}{P_{\text{A}}^{\max} \sigma_v^2 \sum_{n=1}^N |f_n|^2 + \sigma^2 \left( P_{\text{BS}}^{\max} \sum_{n=1}^N |g_n|^2 + N \sigma_v^2 \right)}. \quad (8)$$

Then, assume  $\mathbf{f} \sim \mathcal{CN}(\mathbf{0}_N, \varrho_f^2 \mathbf{I}_N)$  and  $\mathbf{g} \sim \mathcal{CN}(\mathbf{0}_N, \varrho_g^2 \mathbf{I}_N)$ . By letting  $N \rightarrow \infty$  in (8), according to the law of large numbers, we have  $\sum_{n=1}^N |f_n| |g_n| \rightarrow \frac{\pi N \varrho_f \varrho_g}{4}$ ,  $\sum_{n=1}^N |g_n|^2 \rightarrow N \varrho_g^2$ , and  $\sum_{n=1}^N |f_n|^2 \rightarrow N \varrho_f^2$ . Thus, we can further derive the asymptotic SNR of active RISs from (8) as

$$\gamma_{\text{active}} \rightarrow N \frac{P_{\text{BS}}^{\max} P_{\text{A}}^{\max} \pi^2 \varrho_f^2 \varrho_g^2}{16 \left( P_{\text{A}}^{\max} \sigma_v^2 \varrho_f^2 + P_{\text{BS}}^{\max} \sigma^2 \varrho_g^2 + \sigma^2 \sigma_v^2 \right)},$$

which completes the proof.  $\blacksquare$

We can observe from (4) that, compared with the asymptotic SNR of passive RISs [5], i.e.,

$$\gamma_{\text{passive}} \rightarrow N^2 \frac{P_{\text{BS}}^{\max} \pi^2 \varrho_f^2 \varrho_g^2}{16 \sigma^2}, \quad (9)$$

which is proportional to  $N^2$ , the asymptotic SNR of the active RISs,  $\gamma_{\text{active}}$ , is proportional to  $N$  due to the noises additionally introduced by the use of active components. At first glance, it seems that the SNR proportional to  $N^2$  of passive RISs,  $\gamma_{\text{passive}}$ , exceeds the SNR of active RISs,  $\gamma_{\text{active}}$ . However, actually the opposite is true. The reason behind this counterintuitive behavior is that, because of the use of reflection-type amplifiers in active RISs, only when  $N$  is unaffordably large can passive RISs outperform active RISs.

To see the above fact, let us consider two different SISO systems, which are aided by an active RIS and a passive RIS, respectively. Let  $P_{\text{BS-A}}^{\max}$  denote the maximum BS transmit power in the active RIS aided system and  $P_{\text{BS-P}}^{\max}$  denote that in the passive RIS aided system. Then, assuming  $N$  is large, by solving  $\gamma_{\text{passive}} \geq \gamma_{\text{active}}$  according to (4) and (9), the required number of elements  $N$  for passive RISs to outperform active RISs has to satisfy

$$N \geq \frac{P_{\text{BS-A}}^{\max}}{P_{\text{BS-P}}^{\max}} \frac{P_{\text{A}}^{\max} \sigma^2}{\left( P_{\text{A}}^{\max} \sigma_v^2 \varrho_f^2 + P_{\text{BS-A}}^{\max} \sigma^2 \varrho_g^2 + \sigma^2 \sigma_v^2 \right)}. \quad (10)$$

For a fair comparison, we constrain the total transmit power of the two systems by setting  $P_{\text{BS-P}}^{\max} = 2$  W and  $P_{\text{BS-A}}^{\max} =$

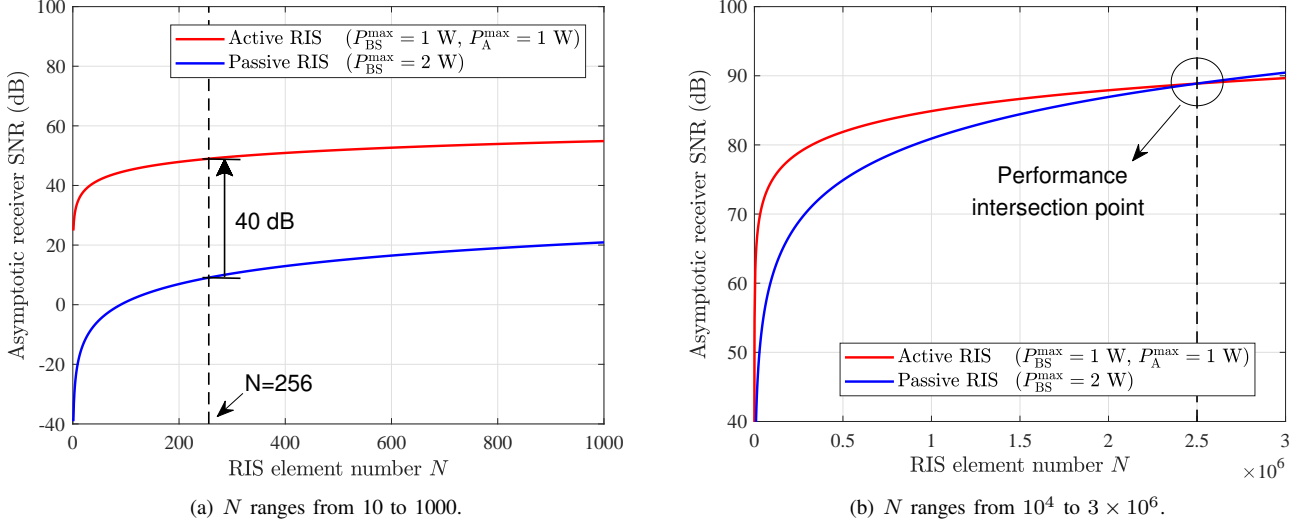


Fig. 3. The simulation results for the asymptotic receiver SNR vs. the number of RIS elements  $N$  with different ranges of  $N$ .

$P_A^{\max} = 1$  W. Therefore, when  $\sigma^2 = \sigma_v^2 = -70$  dBm and  $\varrho_f^2 = \varrho_g^2 = -70$  dB, the required  $N$  is  $2.5 \times 10^6$  according to (10), which is impractical to realize with current technology. Conversely, for a more practical number of elements  $N = 256$ , according to (4) and (9), the SNR achieved by the passive RIS is  $\gamma_{\text{passive}} \approx 9.0$  dB, while the SNR achieved by the active RIS is  $\gamma_{\text{active}} \approx 49.0$  dB, which is about  $10^4$  times higher than  $\gamma_{\text{passive}}$ . To show these results explicitly, we further plot the asymptotic receiver SNR vs. the number of RIS elements  $N$  in Fig. 3, which agrees with our above analyses.

Hence, although additional thermal noise is introduced by the active components, active RISs can still achieve an improved SNR. This is due to the fact that the desired signals reflected by different active RIS elements can be coherently added with the same phase at the user, while the introduced noises cannot.

#### IV. JOINT TRANSMIT BEAMFORMING AND REFLECT PRECODING DESIGN

To investigate the capacity gain of the proposed active RIS in typical wireless systems, in this section, the SISO case studied in Section III is extended to the more general MIMO case. Specifically, we first formulate the sum-rate maximization problem in Subsection IV-A. Then, the proposed joint transmit beamforming and reflect precoding algorithm to solve the problem is introduced in Subsection IV-B. Finally, the convergence and complexity of the proposed algorithm are discussed in IV-C.

##### A. Problem formulation

According to the multi-user MIMO signal model in (3), the signal-to-interference-plus-noise ratio (SINR) at user  $k$  can be derived as

$$\gamma_k = \frac{|\mathbf{H}_k^H \mathbf{w}_k|^2}{\sum_{j=1, j \neq k}^K |\mathbf{H}_k^H \mathbf{w}_j|^2 + \|\mathbf{f}_k^H \mathbf{P} \Theta\|^2 \sigma_v^2 + \sigma^2}, \quad (11)$$

wherein  $\mathbf{H}_k^H = \mathbf{h}_k^H + \mathbf{f}_k^H \mathbf{P} \Theta \mathbf{G} \in \mathbb{C}^{1 \times M}$  is the equivalent channel from the BS to user  $k$ . Therefore, the sum-rate maximization problem can be formulated as follows:

$$\begin{aligned} \max_{\mathbf{W}, \mathbf{P}, \Theta} \quad & R_{\text{sum}} = \sum_{k=1}^K \log_2(1 + \gamma_k) \\ \text{s.t.} \quad & C_1: \sum_{k=1}^K \|\mathbf{w}_k\|^2 \leq P_{\text{BS}}^{\max} \\ & C_2: \sum_{k=1}^K \|\mathbf{P} \Theta \mathbf{G} \mathbf{w}_k\|^2 + \|\mathbf{P} \Theta\|^2 \sigma_v^2 \leq P_A^{\max}, \end{aligned} \quad (12)$$

where  $\mathbf{W} \triangleq [\mathbf{w}_1^T, \dots, \mathbf{w}_K^T]^T$ , while  $C_1$  and  $C_2$  are the power constraints at the BS and active RIS, respectively. Due to the non-convexity of problem (12), the joint design of  $\mathbf{W}$ ,  $\mathbf{P}$ , and  $\Theta$  is challenging. To efficiently solve this problem, we propose a joint beamforming and precoding algorithm based on alternating optimization and fractional programming, as illustrated in the next subsection.

##### B. Proposed joint beamforming and precoding algorithm

Note that, in (12),  $\mathbf{P}$  and  $\Theta$  always appear in product form. In this way,  $\mathbf{P}$  and  $\Theta$  can be merged as  $\Psi = \mathbf{P} \Theta = \text{diag}(p_1 e^{j\theta_1}, \dots, p_N e^{j\theta_N}) \in \mathbb{C}^{N \times N}$ . Then, to deal with the sum-of-logarithm and fractions in (12), we exploit fractional programming [33] to decouple the optimization problem. Specifically, by introducing auxiliary variables  $\rho \triangleq [\rho_1, \dots, \rho_K]$  and  $\varpi \triangleq [\varpi_1, \dots, \varpi_K] \in \mathbb{C}^K$ , the original problem (12) can be equivalently reformulated as follows

$$\begin{aligned} \max_{\mathbf{W}, \Psi, \rho, \varpi} \quad & R'_{\text{sum}}(\mathbf{W}, \Psi, \rho, \varpi) = \sum_{k=1}^K \ln(1 + \rho_k) - \sum_{k=1}^K \rho_k \\ & + \sum_{k=1}^K g_k(\mathbf{W}, \Psi, \rho_k, \varpi_k) \\ \text{s.t.} \quad & C_1: \|\mathbf{W}\|^2 \leq P_{\text{BS}}^{\max} \\ & C_2: \sum_{k=1}^K \|\Psi \mathbf{G} \mathbf{w}_k\|^2 + \|\Psi\|^2 \sigma_v^2 \leq P_A^{\max}, \end{aligned} \quad (13)$$

**Algorithm 1** Proposed joint transmit beamforming and reflect precoding algorithm

---

**Input:** Channels  $\mathbf{G}$ ,  $\mathbf{h}_k$ , and  $\mathbf{f}_k$ ,  $\forall k \in \{1, \dots, K\}$ .  
**Output:** Optimized  $\mathbf{W}$ ,  $\mathbf{P}$ ,  $\Theta$ , and sum-rate  $R_{\text{sum}}$ .  
1: Initialize  $\mathbf{W}$ ,  $\mathbf{P}$  and  $\Theta$ ;  
2: **while** no convergence of  $R_{\text{sum}}$  **do**  
3:   Update  $\rho$  by (14);  
4:   Update  $\varpi$  by (15);  
5:   Update  $\mathbf{W}$  by solving (16);  
6:   Update  $\Psi$  by solving (17);  
7: **end while**  
8: Obtain  $\mathbf{P}$  and  $\Theta$  from  $\Psi$ ;  
9: **return** Optimized  $\mathbf{W}$ ,  $\mathbf{P}$ ,  $\Theta$ , and  $R_{\text{sum}}$ .

---

where

$$g_k(\mathbf{W}, \Psi, \rho_k, \varpi_k) = 2\sqrt{(1 + \rho_k)} \Re \{ \varpi_k^* \mathbf{H}_k^H \mathbf{w}_k \} - |\varpi_k|^2 \left\{ \sum_{j=1}^K |\mathbf{H}_k^H \mathbf{w}_j|^2 + \|\mathbf{f}_k^H \Psi\|^2 \sigma_v^2 + \sigma^2 \right\}.$$

Then, according to the strong convergence of FP methods proved in [33], a locally optimal solution to (13) can be obtained by alternately optimizing  $\mathbf{W}$ ,  $\Psi$ ,  $\rho$ , and  $\varpi$  in (13), until  $R_{\text{sum}}$  converges. For clarity, we summarize the proposed joint beamforming and precoding algorithm in **Algorithm 1**, and the optimal solutions to variables  $\mathbf{W}$ ,  $\Psi$ ,  $\rho$ , and  $\varpi$  are given in the following four steps, respectively.

1) *Step 1: Fix  $(\mathbf{W}, \Psi, \varpi)$  and optimize  $\rho$ :* By solving  $\frac{\partial R'_{\text{sum}}}{\partial \rho_k} = 0$  for (13), the optimal  $\rho$  can be obtained as

$$\rho_k^{\text{opt}} = \frac{\xi_k^2 + \xi_k \sqrt{\xi_k^2 + 4}}{2}, \quad \forall k \in \{1, \dots, K\}, \quad (14)$$

where  $\xi_k = \Re \{ \varpi_k^* \mathbf{H}_k^H \mathbf{w}_k \}$ .

2) *Step 2: Fix  $(\mathbf{W}, \Psi, \rho)$  and optimize  $\varpi$ :* By solving  $\frac{\partial R'_{\text{sum}}}{\partial \varpi_k} = 0$  for (13), the optimal  $\varpi$  is given by

$$\varpi_k^{\text{opt}} = \frac{\sqrt{(1 + \rho_k)} \mathbf{H}_k^H \mathbf{w}_k}{\sum_{j=1}^K |\mathbf{H}_k^H \mathbf{w}_j|^2 + \|\mathbf{f}_k^H \Psi\|^2 \sigma_v^2 + \sigma^2}, \quad \forall k \in \{1, \dots, K\}. \quad (15)$$

3) *Step 3: Fix  $(\Psi, \rho, \varpi)$  and optimize  $\mathbf{W}$ :* By defining

$$\mathbf{b}_k^H = 2\sqrt{(1 + \rho_k)} \varepsilon_k^* \mathbf{H}_k^H, \quad \mathbf{b} = [\mathbf{b}_1^T, \mathbf{b}_2^T, \dots, \mathbf{b}_N^T]^T, \\ \mathbf{A} = \mathbf{I}_K \otimes \sum_{k=1}^K |\varepsilon_k|^2 \mathbf{H}_k \mathbf{H}_k^H, \quad \Xi = \mathbf{I}_K \otimes (\mathbf{G}^H \Psi^H \Psi \mathbf{G}), \\ P_m^{\text{max}} = P_A^{\text{max}} - \|\Psi\|^2 \sigma_v^2,$$

the problem (13) can be reformulated as follows

$$\begin{aligned} \max_{\mathbf{W}} \quad & \Re \{ \mathbf{b}^H \mathbf{W} \} - \mathbf{W}^H \mathbf{A} \mathbf{W} \\ \text{s.t.} \quad & \mathbf{C}_1 : \|\mathbf{W}\|^2 \leq P_{\text{BS}}^{\text{max}} \\ & \mathbf{C}_2 : \mathbf{W}^H \Xi \mathbf{W} \leq P_m^{\text{max}}, \end{aligned} \quad (16)$$

which is a standard quadratic constraint quadratic programming (QCQP) problem. Thus, the optimal  $\mathbf{w}^{\text{opt}}$  can be directly obtained with existing optimization methods such as the alternating direction method of multipliers (ADMM) [34].

4) *Step 4: Fix  $(\mathbf{W}, \rho, \varpi)$  and optimize  $\Psi$ :* By defining  $\psi = [p_1 e^{j\theta_1}, \dots, p_N e^{j\theta_N}]^H$ , where  $\text{diag}(\psi) \triangleq \Psi$ , problem (13) can be reformulated as follows:

$$\begin{aligned} \max_{\psi} \quad & \Re \{ \psi^H \mathbf{v} \} - \psi^H \Omega \psi \\ \text{s.t.} \quad & \mathbf{C}_2 : \psi^H \Pi \psi \leq P_A^{\text{max}}, \end{aligned} \quad (17)$$

wherein

$$\begin{aligned} \mathbf{v} = & 2 \sum_{k=1}^K \sqrt{(1 + \rho_k)} \text{diag}(\varpi_k^* \mathbf{f}_k^H) \mathbf{G} \mathbf{w}_k \\ & - \sum_{k=1}^K |\varpi_k|^2 \text{diag}(\mathbf{f}_k^H) \mathbf{G} \sum_{j=1}^K \mathbf{w}_j \mathbf{w}_j^H \mathbf{h}_k, \\ \Omega = & \sum_{k=1}^K |\varpi_k|^2 \text{diag}(\mathbf{f}_k^H) \text{diag}(\mathbf{f}_k) \sigma_v^2 \\ & + \sum_{k=1}^K |\varpi_k|^2 \sum_{j=1}^K \text{diag}(\mathbf{f}_k^H) \mathbf{G} \mathbf{w}_j \mathbf{w}_j^H \mathbf{G}^H \text{diag}(\mathbf{f}_k), \\ \Pi = & \sum_{k=1}^K \text{diag}(\mathbf{G} \mathbf{w}_k) (\text{diag}(\mathbf{G} \mathbf{w}_k))^H + \sigma_v^2 \mathbf{I}_N. \end{aligned}$$

Note that (17) is also a standard QCQP problem, thus the optimal solution  $\psi^{\text{opt}}$  can be obtained with existing optimization methods such as ADMM [34].

### C. Convergence and complexity discussions

The proposed joint beamforming and precoding algorithm has strict convergency, since each step of the iteration, i.e., (14), (15), (16), and (17), can be easily proved to be monotonous. The overall computational complexity of the proposed algorithm is mainly introduced by the updates of the four variables. Let  $I_a$  and  $I_p$  denote the required iteration numbers for the convergences of problem (16) and (17), respectively. Then, the complexities of updating  $\mathbf{W}$ ,  $\Psi$ ,  $\rho$ , and  $\varpi$  are  $\mathcal{O}(I_a K^2 M^2)$ ,  $\mathcal{O}(I_p N^2)$ ,  $\mathcal{O}(KM)$ , and  $\mathcal{O}(K^2 M + N)$ , respectively. Let  $I_o$  denote the required iteration number for global convergence. Thus, the overall computational complexity for the proposed joint beamforming and precoding algorithm can be approximated by  $\mathcal{O}(I_o (I_a K^2 M^2 + I_p N^2))$ .

## V. VALIDATION RESULTS

In this section, we present experimental results for the developed signal model and simulation results for an active RIS aided MIMO system.

### A. Validation Results for Signal Model

To validate the developed signal model (2), we designed and fabricated an active RIS element with integrated reflection-type amplifier for experimental measurements<sup>2</sup> in [35]. Note that this design can be directly extended to the large-array case [18]. Particularly, since the phase-shifting ability of RISs has been widely verified [18], we focus on studying the reflection

<sup>2</sup>In October 2019, we start to design an active RIS element integrating a reflection-type amplifier. Then, the fabrication of this active RIS element was finished in August 2020. Subsequently, we set out to establish an experimental environment for the signal measurements on this element, and all measurements were completed in February 2021.

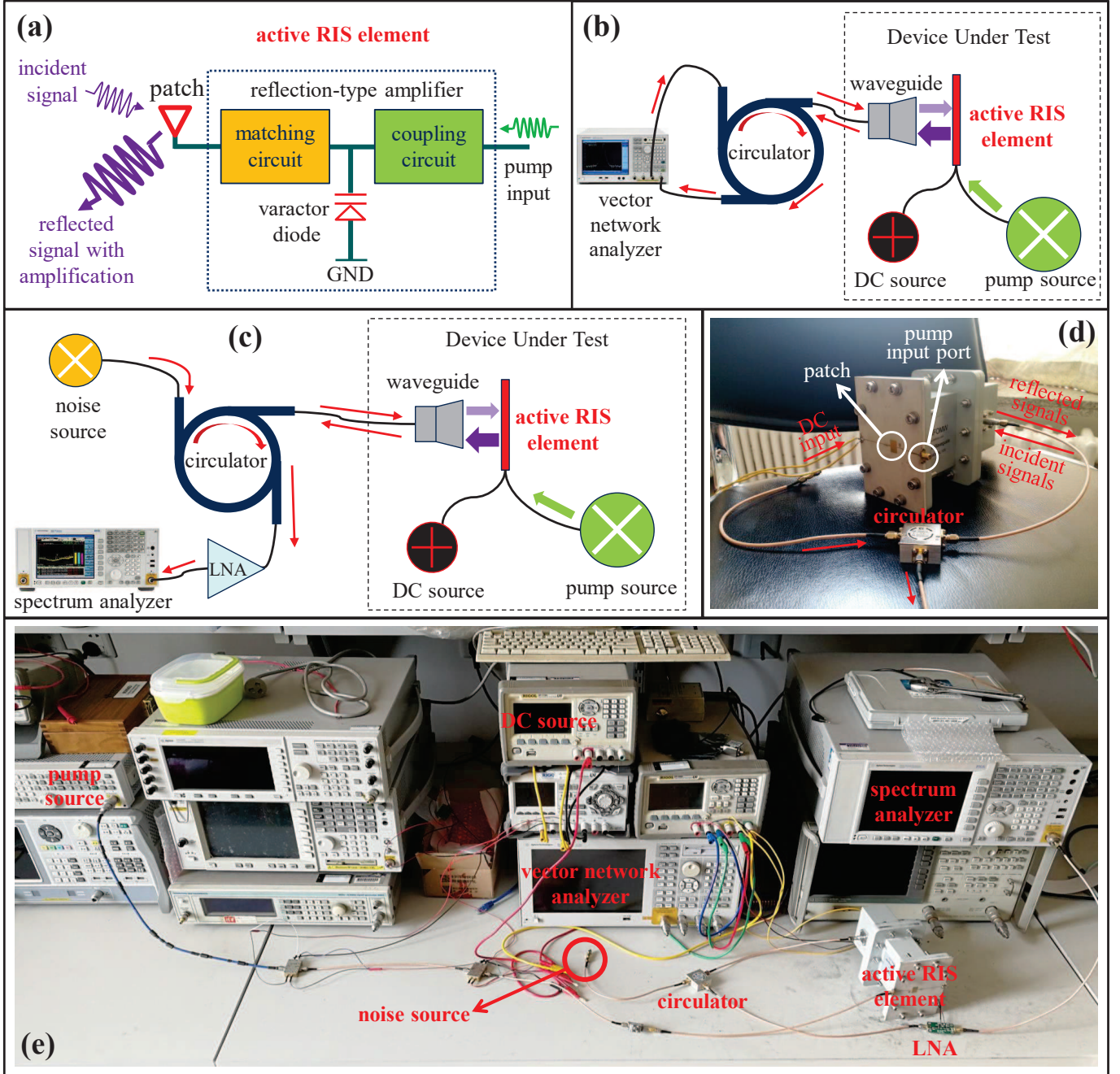


Fig. 4. The experimental devices and environment for validating the developed signal model (2) of the proposed active RIS.

gain and the noise introduced by an active RIS. Thus, the validation of (2) is equivalent to validating

$$P_y = \underbrace{GP_x}_{\text{Desired-signal power}} + \underbrace{G\sigma_v^2 + \sigma_s^2}_{\text{noise power}}, \quad (18)$$

where  $P_y$  is the power of the reflected signals;  $P_x$  is the power of the incident signal;  $p^2 \equiv G$  is the reflection gain of the active RIS element;  $G\sigma_v^2$  and  $\sigma_s^2$  are the dynamic and static noise power at the RIS element, respectively.

To validate the signal model (18), we first establish the systems for experimental measurements as illustrated in Fig. 4. Specifically, Fig. 4 (a) illustrates the structure of the fabricated active RIS element operating at a frequency of 2.36 GHz

[35]. The incident signal and the pump input are coupled in a varactor-diode-based reflection-type amplifier to generate the reflected signal with amplification. Fig. 4 (b) illustrates the system used for measuring the reflection gain of the active RIS element. A direct-current (DC) source is used to provide a bias voltage of 7.25 V for driving the active RIS element, and a pump source is used to control the reflection gain. A circulator is used to separate the incident signal and the reflected signal, and the reflection gain is directly measured by a vector network analyzer. Fig. 4 (c) illustrates the system for measuring the noises introduced at the active RIS element, where a spectrum analyzer is used to measure the noise power. The noise source is a 50  $\Omega$  impedance for simulating an

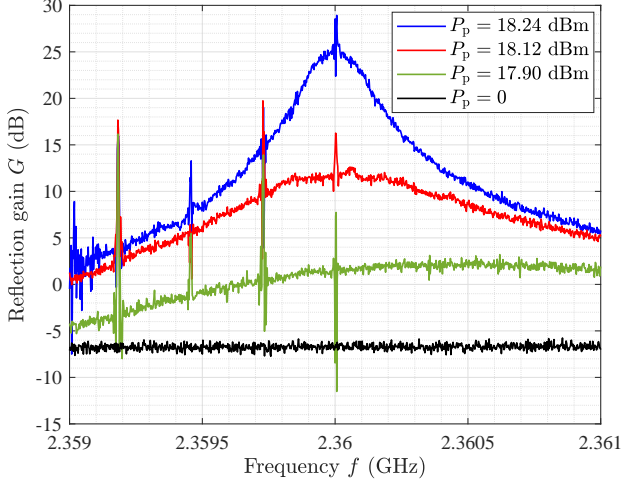
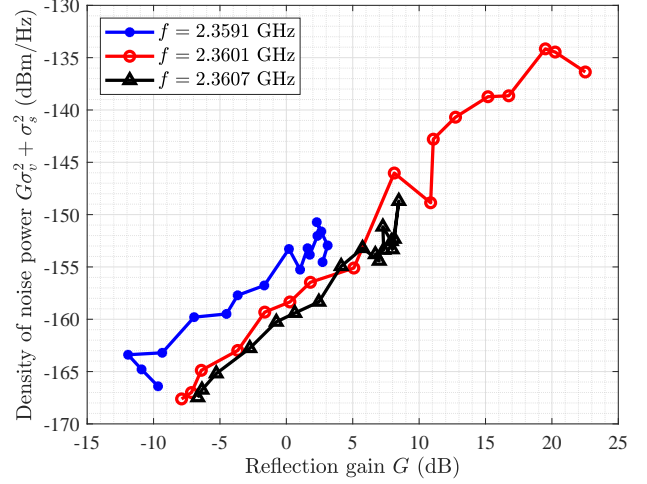
(a) Reflection gain  $G$  vs. signal frequency  $f$ .(b) Density of noise power  $G\sigma_v^2 + \sigma_s^2$  vs. reflection gain  $G$ .

Fig. 5. The experimental measurement results for the signal model of an active RIS.

input noise of -174 dBm/Hz at each patch. The reflected signal is amplified by a low-noise amplifier (LNA) so that the spectrum analyzer can detect it. Fig. 4 (d) shows a photo of the fabricated active RIS element under test, which is connected by a waveguide for signal exchanges. Fig. 4 (e) is a photo of the experimental environment with the required equipment for device driving and signal measurement.

Using the measurement system for the reflection gain depicted in Fig. 4 (b), we first investigate the reflection gain  $G$  of the active RIS element. Note that the reflection gain  $G$  is controlled by the input power of the pump source  $P_p$ . By setting the input power of the vector network analyzer as  $P_x = -50$  dBm, the reflection gain  $G$  as a function of the signal frequency can be directly measured via the vector network analyzer. Then, in Fig. 5 (a), we show the measurement results for the reflection gain  $G$  as a function of the signal frequency  $f$  and for different powers of the pump source  $P_p$ . We can observe that the active RIS element can achieve a reflection gain,  $G$ , of more than 25 dB, when  $P_p = 18.24$  dBm, which confirms the significant reflection gains enabled by active RISs. On the other hand, when  $P_p = 0$ ,  $G$  falls to -6 dB, which is lower than the expected 0 dB. This result is caused by the inherent power losses of the circulator and transmission lines used for measurement.

We further study the noise power introduced by the active RIS element, i.e.,  $G\sigma_v^2 + \sigma_s^2$  in (18). Using the noise measurement system in Fig. 4 (c), in Fig. 5 (b), we show the measurement results for the spectral density of noise power  $G\sigma_v^2 + \sigma_s^2$  as a function of  $G$  for different operating frequencies. We can observe that the noise power increases nearly linearly with  $G$ , which verifies the noise model  $G\sigma_v^2 + \sigma_s^2$  in (18). Particularly, for  $f = 2.3601$  GHz, the spectral density of  $\sigma_s^2$  is about -174 dBm/Hz, while that of  $\sigma_v^2$  is about -160 dBm/Hz, which is about 15 dB higher. The reason for this is that the input noise is amplified by the noise factor [23], and additional noises are also introduced by the other active devices in our measurements, such as the leakage noise from the DC source.

### B. Simulation Results for Joint Precoding Design

To evaluate the performance of the proposed active RIS in typical wireless systems, in this subsection, we present simulation results for an active RIS aided MIMO system.

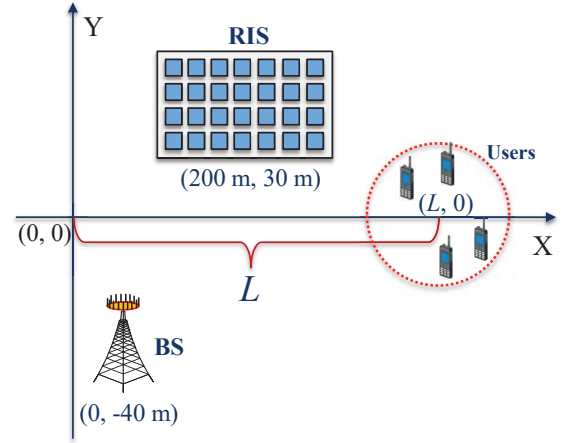
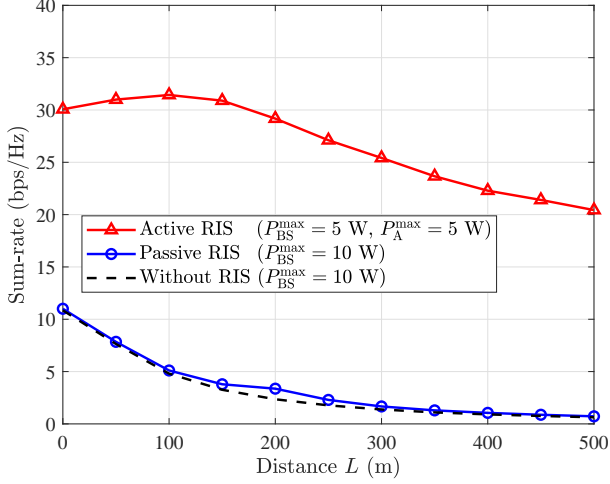


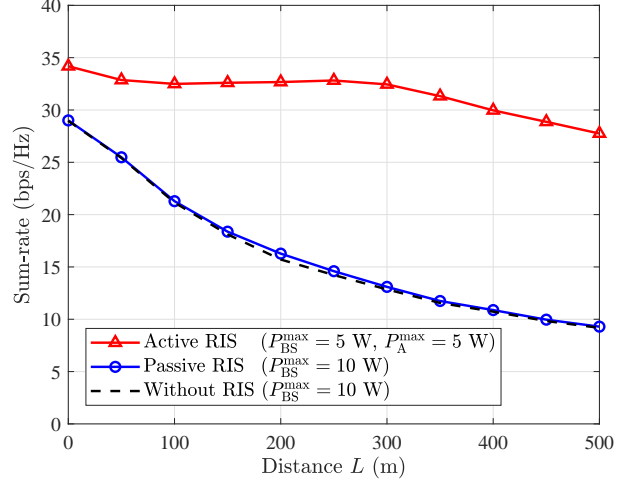
Fig. 6. The simulation scenario where a BS aided by an active RIS serves four users.

TABLE I  
SIMULATION PARAMETERS.

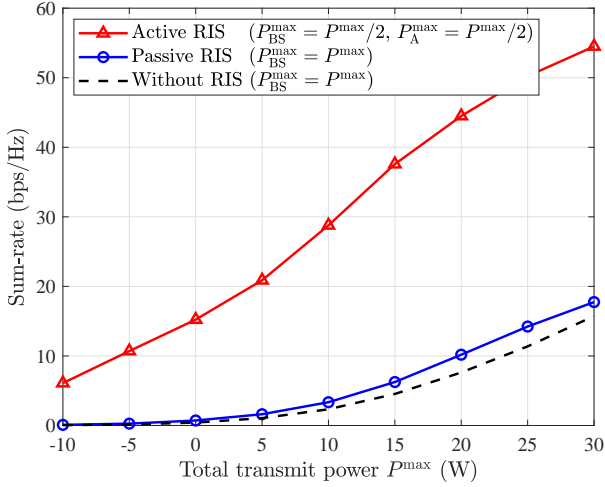
System parameters	Values
Operation frequency	$f = 5$ GHz
Antenna/element spacing	Half wavelength
BS antenna number	$M = 4$
RIS element number	$N = 256$
User number	$K = 4$
BS location	$(0, -40$ m)
RIS location	$(200$ m, $30$ m)
Center of user locations	$(L, 0)$
Total transmit power	$P^{\max} = 10$ W
Noiser power	$\sigma^2 = \sigma_v^2 = -70$ dBm



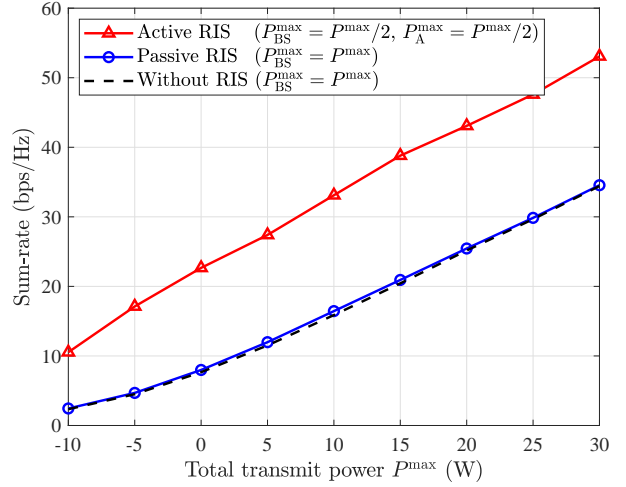
(a) Sum-rate in scenario 1 without an LoS direct link.



(b) Sum-rate in scenario 2 with an LoS direct link.

Fig. 7. Simulation results for the sum-rate vs. distance  $L$  in an RIS-aided MIMO system.

(a) Sum-rate in scenario 1 without an LoS direct link.



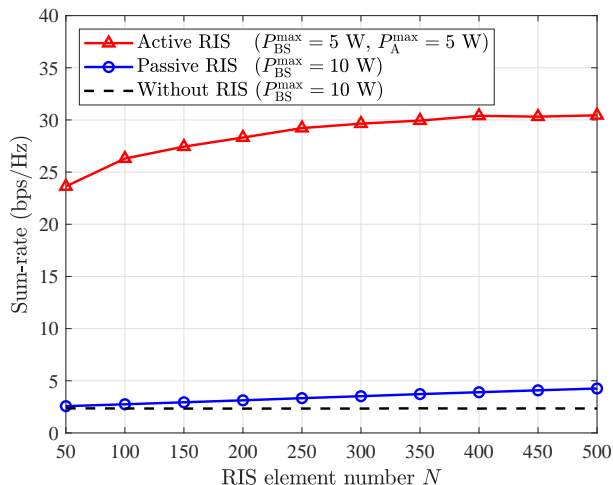
(b) Sum-rate in scenario 2 with an LoS direct link.

Fig. 8. Simulation results for the sum-rate vs. the total transmit power  $P^{\max}$  in an RIS-aided MIMO system.

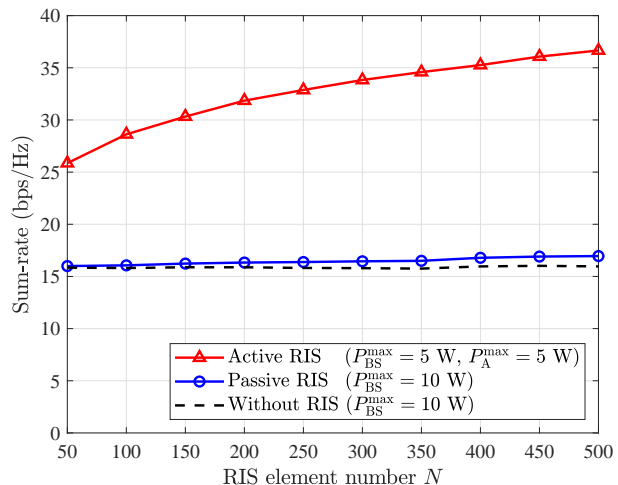
For the simulation setup, we consider an active RIS aided MIMO system as shown in Fig. 6. The BS and the active/passive RIS are located at  $(0, -40 \text{ m})$  and  $(200 \text{ m}, 30 \text{ m})$ , respectively. The four users are randomly located in a circle with a radius of 5 m from the center  $(L, 0)$ . The free-space model [17] with Rayleigh small-scale fading is used to generate all channels. To characterize the case when the direct link is blocked, we assume that the channel gain of the blocked link is 1% of that of the unobstructed line-of-sight (LoS). [9]. The other parameter settings are summarized in Table I. For fair comparison, we constrain the total transmit power  $P^{\max}$  to 10 W by setting  $P_{\text{BS}}^{\max} = P_{\text{A}}^{\max} = 5 \text{ W}$  for the active RIS aided system and  $P_{\text{BS}}^{\max} = 10 \text{ W}$  for the benchmark systems. For the active RIS, the proposed **Algorithm 1** is employed, while for the passive RIS, an existing algorithm in [21] is used.

For comparison, we consider two scenarios with different channel conditions. For both scenarios, the BS-RIS-user re-

flection links are LoS, while the BS-user direct links are blocked in scenario 1 and LoS in scenario 2, respectively. Then, in Fig. 7 (a) and (b), we plot the sum-rate vs. distance  $L$  in the two scenarios, respectively. From these results, we have two observations. Firstly, in scenario 1 without an LoS direct link, the passive RIS can indeed achieve a performance improvement, while the active RIS achieves a much higher sum-rate gain. Secondly, in scenario 2 with an LoS direct link, the passive RIS achieves only a negligible sum-rate gain, while the active RIS can still realize a noticeable sum-rate gain. For example, when  $L = 200 \text{ m}$ , the capacities without RIS, with passive RIS, and with active RIS in scenario 1 are 2.35 bps/Hz, 3.37 bps/Hz, and 29.18 bps/Hz respectively, while in scenario 2, these values are 15.71 bps/Hz, 16.27 bps/Hz, and 32.67 bps/Hz, respectively. At this position, the passive RIS provides a 43% gain in scenario 1 and a negligible 3% gain in scenario 2. By contrast, active RIS can achieve noticeable



(a) Sum-rate in scenario 1 without an LoS direct link.



(b) Sum-rate in scenario 2 with an LoS direct link.

Fig. 9. Simulation results for the sum-rate vs. the RIS element number  $N$  in an RIS-aided MIMO system.

sum-rate gains of 1142% in scenario 1 and 108% in scenario 2, which are much higher than those achieved by the passive RIS in the corresponding scenarios. These results demonstrate that, compared with the existing passive RIS, the proposed active RIS can overcome the “multiplicative fading” effect and achieve noticeable sum-rate gains in both communication scenarios.

### C. The impact of key parameters on system performances

To reveal more insights of the proposed active RIS, in this subsection we study the impact of key parameters on system performances.

By considering the same simulation setup in Subsection V-B and fixing the distance as  $L = 200$  m, we plot the users’ sum-rate vs. the total transmit power  $P^{\max}$  in Fig. 8. For scheme “Active RIS”, we assume the total transmit power  $P^{\max}$  is equally allocated to the BS and the active RIS for a fair comparison. From these two subfigures we observe that, the passive RIS only achieves visible performance gains in scenario 1 where the direct link is LoS, while in scenario with an LoS direct link, the passive RIS achieves negligible sum-rate gain. By contrast, in both scenarios, the active RIS realizes a high performance gain. Particularly, we note that, the performance gap between the curves “Passive RIS” and “Active RIS” becomes larger as the transmit power increases. It is because, for scheme “Passive RIS”, the total transmit power is only allocated to the BS, thus all transmit power suffers path loss twice. However, for scheme “Active RIS”, half of the transmit power is allocated to the active RIS, and this transmitted power by active RIS only suffers path loss once. It implies that, the total power loss of the active RIS aided system is lower than that of the passive RIS aided system, thus the proposed active RIS is also promising to reduce the required transmit power in communication systems, which can be investigated in follow-up works.

Then, under the same setup, we plot the users’ sum-rate vs. the RIS element number  $N$  in Fig. 9. From these two

subfigures, we can observe that, as the RIS element number  $N$  increases, both the passive RIS and the active RIS can achieve higher sum-rate gain, while the performance improvement of the active RIS is greater than that of the passive RIS. For example, when the number of RIS elements  $N$  increases from 50 to 500, the sum-rate of passive RIS aided system increases from 2.57 bps/Hz to 4.26 bps/Hz in scenario 1 and from 15.99 bps/Hz to 16.95 bps/Hz in scenario 2. By contrast, the sum-rate of active RIS aided system increases from 23.63 bps/Hz to 30.44 bps/Hz in scenario 1 and from 25.86 bps/Hz to 36.66 bps/Hz in scenario 2, which increases faster than that of the passive RIS aided system. It indicates that, when the element number  $N$  is not too large (such as millions of elements), compared with the passive RIS, increasing the element number of the active RIS is more efficient to improve the system capacity, which agrees with the performance analysis in Section III.

## VI. CONCLUSIONS

In this paper, we have proposed the concept of active RISs to overcome the fundamental limitation of the “multiplicative fading” effect. Then, we have developed a signal model for active RISs, which has been validated by a fabricated active RIS element through experimental measurements. Based on the proposed signal model, we have analyzed the capacity gain achievable by active RISs and then formulated an optimization problem to maximize the users’ sum-rate in an active RIS aided MIMO system. Subsequently, we have proposed a joint transmit beamforming and reflect precoding algorithm to solve this problem. Finally, experimental and simulation results have shown that, compared with the benchmark scheme without RIS, the existing passive RIS can realize only a negligible sum-rate gain of about 3% in a typical application scenario, while the proposed active RIS can achieve a noticeable sum-rate gain of about 108%, thus indeed overcoming the fundamental limitation of the “multiplicative fading” effect.

## REFERENCES

- [1] L. Zhang, X. Q. Chen, S. Liu, Q. Zhang, J. Zhao, J. Y. Dai, G. D. Bai, X. Wan, Q. Cheng, G. Castaldi, V. Galdi, and T. J. Cui, "Space-time-coding digital metasurfaces," *Nat. Commun.*, vol. 9, no. 4338, Oct. 2018.
- [2] X. Ni, A. V. Kildishev, and V. M. Shalaev, "Metasurface holograms for visible light," *Nat. Commun.*, vol. 4, no. 2807, Nov. 2013.
- [3] H. Ren, "A light-programmable metasurface," *Nat. Elect.*, vol. 3, pp. 137–138, Mar. 2020.
- [4] S. Venkatesh, X. Lu, H. Saeidi, and K. Sengupta, "A high-speed programmable and scalable terahertz holographic metasurface based on tiled CMOS chips," *Nat. Elect.*, vol. 3, pp. 785–793, Dec. 2020.
- [5] M. Di Renzo, A. Zappone, M. Debbah, M. S. Alouini, C. Yuen, J. de Rosny, and S. Tretyakov, "Smart radio environments empowered by reconfigurable intelligent surfaces: How it works, state of research, and the road ahead," *IEEE J. Sel. Areas Commun.*, vol. 38, no. 11, pp. 2450–2525, Nov. 2020.
- [6] E. Basar, M. Di Renzo, J. De Rosny, M. Debbah, M. Alouini, and R. Zhang, "Wireless communications through reconfigurable intelligent surfaces," *IEEE Access*, vol. 7, pp. 116753–116773, Aug. 2019.
- [7] L. Dai, B. Wang, M. Wang, X. Yang, J. Tan, S. Bi, S. Xu, F. Yang, Z. Chen, M. Di Renzo, C. B. Chae, and L. Hanzo, "Reconfigurable intelligent surface-based wireless communications: Antenna design, prototyping, and experimental results," *IEEE Access*, vol. 8, pp. 45913–45923, Mar. 2020.
- [8] C. Huang, R. Mo, and C. Yuen, "Reconfigurable intelligent surface assisted multiuser MISO systems exploiting deep reinforcement learning," *IEEE J. Sel. Areas Commun.*, vol. 38, no. 8, pp. 1839–1850, Aug. 2020.
- [9] P. Wang, J. Fang, X. Yuan, Z. Chen, and H. Li, "Intelligent reflecting surface-assisted millimeter wave communications: Joint active and passive precoding design," *IEEE Trans. Veh. Technol.*, vol. 69, no. 12, pp. 14960–14973, Dec. 2020.
- [10] C. Huang, A. Zappone, G. C. Alexandropoulos, M. Debbah, and C. Yuen, "Reconfigurable intelligent surfaces for energy efficiency in wireless communication," *IEEE Trans. Wireless Commun.*, vol. 18, no. 8, pp. 4157–4170, Aug. 2019.
- [11] H. Zhao, Y. Shuang, M. Wei, T. J. Cui, P. Hougne, and L. Li, "Metasurface-assisted massive backscatter wireless communication with commodity Wi-Fi signals," *Nat. Commun.*, vol. 11, no. 3926, Aug. 2020.
- [12] M. Faraji-Dana, E. Arbabi, A. Arbabi, S. M. Kamali, H. Kwon, and A. Faraon, "Compact folded metasurface spectrometer," *Nat. Commun.*, vol. 9, no. 4196, Oct. 2013.
- [13] J. Park, B. G. Jeong, S. I. Kim, D. Lee, J. Kim, C. Shin, C. B. Lee, T. Otsuka, J. Kyoung, S. Kim, K. Yang, Y. Park, J. Lee, I. Hwang, J. Jang, S. H. Song, M. L. Brongersma, K. Ha, S. Hwang, H. Choo, and B. L. Choi, "All-solid-state spatial light modulator with independent phase and amplitude control for three-dimensional LiDAR applications," *Nat. Nanotechnol.*, vol. 16, p. 69–76, Oct. 2020.
- [14] W. Zhao, G. Wang, S. Atapattu, T. A. Tsiftsis, and C. Tellambura, "Is backscatter link stronger than direct link in reconfigurable intelligent surface-assisted system?" *IEEE Commun. Lett.*, vol. 24, no. 6, pp. 1342–1346, Jun. 2020.
- [15] T. Hou, Y. Liu, Z. Song, X. Sun, and Y. Chen, "MIMO-NOMA networks relying on reconfigurable intelligent surface: A signal cancellation-based design," *IEEE Trans. Commun.*, vol. 68, no. 11, pp. 6932–6944, Nov. 2020.
- [16] Z. Zhang and L. Dai, "A joint precoding framework for wideband reconfigurable intelligent surface-aided cell-free network," *IEEE Trans. Signal Process.*, Jun. 2020.
- [17] M. Najafi, V. Jamali, R. Schober, and H. V. Poor, "Physics-based modeling and scalable optimization of large intelligent reflecting surfaces," *IEEE Trans. Commun.*, vol. 69, no. 4, pp. 2673–2691, Apr. 2021.
- [18] H. Yang, F. Yang, X. Cao, S. Xu, J. Gao, X. Chen, M. Li, and T. Li, "A 1600-element dual-frequency electronically reconfigurable reflectarray at x/ku-band," *IEEE Trans. Antennas Propag.*, vol. 65, no. 6, pp. 3024–3032, Jun. 2017.
- [19] D. Headland, T. Niu, E. Carrasco, D. Abbott, S. Sriram, M. Bhaskaran, C. Fumeaux, and W. Withayachumnankul, "Terahertz reflectarrays and nonuniform metasurfaces," *IEEE J. Sel. Topics Quantum Electron.*, vol. 23, no. 4, pp. 1–18, Aug. 2017.
- [20] C. Hu, L. Dai, S. Han, and X. Wang, "Two-timescale channel estimation for reconfigurable intelligent surface aided wireless communications," *IEEE Trans. Commun.*, Apr. 2021.
- [21] C. Pan, H. Ren, K. Wang, W. Xu, M. El-kashlan, A. Nallanathan, and L. Hanzo, "Multicell MIMO communications relying on intelligent reflecting surfaces," *IEEE Trans. Wireless Commun.*, vol. 19, no. 8, pp. 5218–5233, Aug. 2020.
- [22] J. Lončar, Z. Šipuš, and S. Hrabar, "Ultrathin active polarization-selective metasurface at X-band frequencies," *Physical Review B*, vol. 100, no. 7, p. 075131, Oct. 2019.
- [23] J. Bousquet, S. Magierowski, and G. G. Messier, "A 4-GHz active scatterer in 130-nm CMOS for phase sweep amplify-and-forward," *IEEE Trans. Circuits Syst. I*, vol. 59, no. 3, pp. 529–540, Mar. 2012.
- [24] K. K. Kishor and S. V. Hum, "An amplifying reconfigurable reflectarray antenna," *IEEE Trans. Antennas Propag.*, vol. 60, no. 1, pp. 197–205, Jan. 2012.
- [25] X. Mu, Y. Liu, L. Guo, J. Lin, and R. Schober, "Simultaneously transmitting and reflecting (STAR) RIS aided wireless communications," *arXiv preprint arXiv:2104.01421*, Apr. 2021.
- [26] Y. Liu, X. Mu, J. Xu, R. Schober, Y. Hao, H. V. Poor, and L. Hanzo, "STAR: Simultaneous transmission and reflection for 360° coverage by intelligent surfaces," *arXiv preprint arXiv:2103.09104*, Mar. 2021.
- [27] S. Zeng, H. Zhang, B. Di, Y. Tan, Z. Han, H. V. Poor, and L. Song, "Reconfigurable intelligent surfaces in 6G: Reflective, transmissive, or both?" *IEEE Commun. Lett.*, vol. 25, no. 6, pp. 2063–2067, Jun. 2021.
- [28] J. He, N. T. Nguyen, R. Schroeder, V. Tapio, J. Korkkonen, and M. Juntti, "Channel estimation and hybrid architectures for RIS-assisted communications," *arXiv preprint arXiv:2104.07115*, Apr. 2021.
- [29] N. T. Nguyen, Q.-D. Vu, K. Lee, and M. Juntti, "Hybrid relay-reflecting intelligent surface-assisted wireless communication," *arXiv preprint arXiv:2103.03900*, Mar. 2021.
- [30] E. Basar, "Transmission through large intelligent surfaces: A new frontier in wireless communications," in *Proc. European Conf. Netw. Commun. (EuCNC'19)*, Jun. 2019, pp. 1–6.
- [31] K. Ntontin, J. Song, and M. D. Renzo, "Multi-antenna relaying and reconfigurable intelligent surfaces: End-to-end SNR and achievable rate," *arXiv preprint arXiv:1908.07967*, Aug. 2019.
- [32] X. Qian, M. Di Renzo, J. Liu, A. Kammoun, and M. S. Alouini, "Beamforming through reconfigurable intelligent surfaces in single-user MIMO systems: SNR distribution and scaling laws in the presence of channel fading and phase noise," *IEEE Wireless Commun. Lett.*, vol. 10, no. 1, pp. 77–81, Jan. 2021.
- [33] K. Shen and W. Yu, "Fractional programming for communication systems—part I: Power control and beamforming," *IEEE Trans. Signal Process.*, vol. 66, no. 10, pp. 2616–2630, May 2018.
- [34] S. Boyd, N. Parikh, E. Chu, B. Peleato, and J. Eckstein, "Distributed optimization and statistical learning via the alternating direction method of multipliers," Nov. 2014, [Online] Available: [https://stanford.edu/~boyd/papers/pdf/admm\\_distr\\_stats.pdf](https://stanford.edu/~boyd/papers/pdf/admm_distr_stats.pdf).
- [35] X. Chen and F. Yang, "Nonlinear electromagnetic surfaces: Theory, design and application," *Master Thesis in Tsinghua University*, May 2020, [Online] Available: <http://etds.lib.tsinghua.edu.cn/Thesis>.